Fast 3D Scene Alignment with Stereo Images using a Stixel-based 3D Model

Dennis W. J. M. van de Wouw[1,2], Willem P. Sanberg[1], Gijs Dubbelman[1] and Peter H. N. de With[1]
[1]*Department of Electrical Engineering, Eindhoven University of Technology, Eindhoven, The Netherlands*
[2]*ViNotion B.V., Eindhoven, The Netherlands*

Keywords: Image Registration, Real-time, View Synthesis, Stixel-World.

Abstract: Scene alignment for images recorded from different viewpoints is a challenging task, especially considering strong parallax effects. This work proposes a diorama-box model for a 2.5D hierarchical alignment approach, which is specifically designed for image registration from a moving vehicle using a stereo camera. For this purpose, the Stixel World algorithm is used to partition the scene into super-pixels, which are transformed to 3D. This model is further refined by assigning a slanting orientation to each stixel and by interpolating between stixels, to prevent gaps in the 3D model. The resulting alignment shows promising results, where under normal viewing conditions, more than 96% of all annotated points are registered with an alignment error up to 5 pixels at a resolution of 1920×1440 pixels, executing at near-real time performance (4 fps) for the intended application.

1 INTRODUCTION

Image registration is the process of placing two images captured from different viewpoints in the same coordinate system. It ensures that pixels representing the same world point in both images, map to the same image coordinates after successful registration. This is relevant in many applications, such as medical image analysis, object recognition, image stitching and change detection (van de Wouw et al., 2016). Especially for the latter application, an accurate alignment is crucial as it enables pixel-wise comparisons between the two images.

Image registration becomes quite challenging when considering images acquired from a moving vehicle in an urban environment, which is the focus of this work. In a repetitive capturing scenario, images are typically acquired from different viewpoints, while significant time may have passed between capturing the historic image and the live image. This poses additional challenges, where the registration now has to cope with dynamic appearance changes of the scene, as well as strong parallax effects.

Appearance changes are generally unavoidable when recording outdoors at different moments in time. Changes in lighting and different weather conditions may significantly affect the colors and contrast of a scene. Furthermore, there may be dynamic changes in the scene, such as other traffic participants and objects placed in or removed from the scene in between the recordings moments. Although such an object may only exist in either the historic image or the live image, it should still be aligned to the correct part of the other image. As a result, regular flow-based methods cannot be used to align such objects as they are not present in both images (Werlberger et al., 2010).

Another challenge is parallax, which results in a difference between the apparent positions of an object viewed along two different lines of sight, e.g. when images are captured from different viewpoints. As a consequence, the relative position and even the ordering of objects in the historic and live image may change when capturing the same scene from two different viewpoints. This is depicted in Figure 1, where the object ordering changes from A-B-C-D to A-C-B-D. This change in relative positions of the objects, depending on their 3D position in the scene, can no longer be handled by a global-affine transformation of the images.

To overcome the parallax issue, the registration problem can be solved in 3D, where the positioning of objects is uniquely defined. By aligning the 3D point clouds and projecting the results back to 2D, parallax is handled correctly. However, since our 3D points are estimated from a stereo camera using dis-

Wouw, D., Sanberg, W., Dubbelman, G. and With, P.
Fast 3D Scene Alignment with Stereo Images using a Stixel-based 3D Model.
DOI: 10.5220/0006535302500259
In *Proceedings of the 13th International Joint Conference on Computer Vision, Imaging and Computer Graphics Theory and Applications (VISIGRAPP 2018) - Volume 4: VISAPP*, pages 250-259
ISBN: 978-989-758-290-5

Figure 1: Sample images showing the same scene from different viewpoints. Note the perspective distortion and the parallax effect, i.e. the same lighting pole *C* is located in front of *A* in the left image, while it is in front of *B* in the right image.

parity estimation, they are not sufficiently accurate for a direct projection. Instead, a model-based projection is required that is robust against noise in the 3D-point cloud. For this purpose and as an initial step, we adopt the hierarchical 2.5D alignment approach introduced in (van de Wouw et al., 2016), which is explained in Section 3. This adopted approach is only able to align the non-linear ground surface, but not the objects above the ground surface. Therefore and as a next step, the main focus of this work is to extend the alignment to the entire scene, including 3D objects.

The remainder of this paper is organized as follows. In the next section, the proposed method is laid out to related work on image registration under viewpoint differences and 3D scene modeling. Section 3 summarizes the baseline image registration method. Section 4 details the proposed method, followed by a validation of our method in Section 5. A discussion on the application of the proposed work is given in Section 6. Finally, Section 7 presents conclusions.

2 RELATED WORK

2.1 Image Registration under Viewpoint Differences

To handle perspective distortion during alignment of images from different viewpoints, several approaches exist. The first approach involves segmenting the 2D scene into sufficiently small parts, such that for each part an individual affine transformation exists to register it to the target image or to a common coordinate system. For this purpose, the authors of (Zhang et al., 2016) and (Su and Lai, 2015) use a mesh-based approach, where they divide the image into a grid and for each cell find a local affine transformation. This way, they can accommodate moderate deviations from planar structures. Lou and Gevers (Lou and Gevers, 2014) first segment the scene into planar regions and find an affine transformation for every plane, in theory allowing to prevent the parallax issues illustrated in Figure 1. Although these methods show promising results, they cannot be performed in real-time, making them less suited to be used while driving, which is the aim of our work.

Another approach is to solve the alignment in 3D. As a change in viewpoint does not alter the relative 3D positions of the objects in the scene, the problem simplifies to estimating a rigid transformation. The aligned 3D point cloud is then projected back to 2D, such that the historic scene is rendered from the live camera viewpoint. The naive approach would transform each individual point in the point cloud and project it to 2D separately. However, this causes significant holes in the resulting image, which become more apparent when viewpoint differences are considered. Alternatively, a hierarchical 2.5D alignment (van de Wouw et al., 2016) can be employed. This method applies a rigid 3D transformation to a textured polygon model of the historic scene, after which the transformed model is projected back to 2D. This results in a registered image without holes in which parallax is handled correctly, i.e. the objects are in the correct positions in the 2D image. Moreover, this strategy allows for real-time execution while driving. For this reason, we build further upon this method in our current work.

2.2 3D Scene Modeling

Projecting textured surfaces outperforms per-pixel processing, since it facilitates addressing holes and noise in the depth data. For this purpose, we require a 3D surface model for the full scene. In the field of 3D reconstruction, meshes are a common data representation. These meshes are often acquired via a Delaunay triangulation of measured point clouds. Typically, these algorithms aim at single object reconstruction (such as digitizing statues and the like, for cultural preservation), but several methods are also employed in our context: outdoor scene modeling. These systems achieve a high level of geometric accuracy in the data that is captured close to the objects in the scene, e.g. facade modeling with accurate ridges and window stills, etc. (Salman and Yvinec, 2010) (Chauve et al., 2010), or detailed rock-mass-surface and staircases (Maiti and Chakravarty, 2016). However, the processing times of these algorithms lies in the order of seconds (Salman and Yvinec, 2010) (Maiti and Chakravarty, 2016) or even minutes (Labatut et al., 2009) (Chauve et al., 2010) per scene, which does not satisfy our real-time processing constraints. Moreover, our system does not need that level of detail. Faster pipelines exist, but typically provide 3D models that are too sparse or coarse (Natour et al., 2015),

whereas we need dense modeling.

Alternative modeling strategies can be derived from algorithms that are predominantly designed for image segmentation instead of 3D modeling, namely: super-pixel methods. In general, they have been designed to process 2D color images, such as LV (Felzenszwalb and Huttenlocher, 2004), SLIC (Achanta et al., 2012) and SEOF (Veksler et al., 2010). Each of these has its own various extensions to incorporate 2.5D or point cloud data. Extensions for LV involve LVPCS (Strom et al., 2010), MLVS (Sanberg et al., 2013) and GBIS+D (Cordts et al., 2016), SLIC is extended in StereoSLIC (Yamaguchi et al., 2014), and SEOF is modified into SEOF+D (Cordts et al., 2016). Although all of these methods can provide relevant super-pixel segmentations, the resulting super-pixels are shaped irregularly, yielding an inefficient representation. Moreover, they need to be calculated on the whole image at once. For trading off modeling flexibility versus optimality and computational complexity, the Stixel World has been introduced (Pfeiffer, 2012). This probabilistic super-pixel method has been designed specifically for the context of intelligent vehicles, aiming at providing a compact yet robust representation of traffic scenes in front of a vehicle, which can be generated efficiently in real time. The Stixel World algorithm relies on disparity data to partition scenes into vertically stacked, rectangular patches of a certain height and 3D position with respect to the camera sensor. These rectangular patches are labeled as either ground or obstacle during the segmentation process, thereby providing a semantic segmentation as well as a 3D representation. Moreover, stixels can be computed efficiently using Dynamic Programming, where multiple columns of disparity measurements are processed in parallel (Pfeiffer, 2012).

Another specialized scene modeling method for intelligent vehicles relies on 3D voxels (Broggi et al., 2013). It generates and removes cubic voxels to handle the dynamic aspect of a traffic scene and stores them efficiently in an octree-based fashion. However, it relies on tracking the voxels over time and does not employ any real-world regularization. Since our system operates at a low frame rate ($\pm$6 fps), but at a much higher resolution (above HD instead of VGA), this method is likely to provide noisy and spurious false detections.

Considering the methods described above, we propose to avoid modeling of the entire scene into an expensive detailed mesh, or in a voxel grid without strict regularization. Instead, we introduce a simplified 3D model, which we refer to as the 'diorama-box model', shown in Figure 3. This model extends the non-linear surface model from (van de Wouw et al., 2016) with 3D objects, where objects are modeled by one or more slanted planar regions (in 3D) estimated from a Stixel World representation. The proposed model allows for real-time computation.

The main contributions of this paper are as follows. First, we introduce an efficient 3D scene model to be used in the 2.5D hierarchical alignment approach (van de Wouw et al., 2016), by including super-pixels obtained through the Stixel World algorithm into the existing ground model. Second, we improve the consistency of the 3D model by adapting the obtained stixel-based model. Finally, we validate the proposed model by employing it in our scene-alignment approach and generally show that the registration error is below 5 pixels for HD+ images (1920×1440 pixels).

3 BASELINE IMAGE REGISTRATION

The 2.5D hierarchical alignment approach (van de Wouw et al., 2016) aims at aligning two images of the same scene that are captured from different viewpoints. It builds on the idea that registration errors due to parallax can be avoided when aligning the 3D point clouds, instead of directly transforming the 2D images. For this purpose, a 3D scene model of the historic scene is constructed onto which the historic texture is projected. Next, this textured model is transformed to the coordinate system of the live image. The transformed model is then projected back to 2D, which renders the historic image as if seen by the live camera. Finally, small misalignments after initial registration are corrected by a registration refinement based on optical flow. This approach is summarized in Figure 2.

The 3D transformation (pose) estimation from Figure 2 lies outside the scope of this paper and is described in more detail in (van de Wouw et al., 2017). The current work focuses on the 3D scene reconstruction and aims at registering the historic image to the live image in 2D.

It should be noted that we are not necessarily interested in 3D model accuracy, as long as the model is able to simulate the 2D aligned image with a low registration error. In a similar fashion, the pose estimation also minimizes the registration error after projection to 2D, instead of establishing the 3D pose in world coordinates.

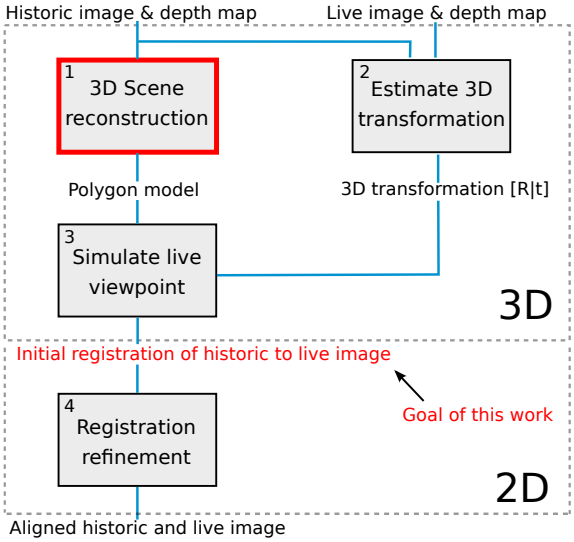

Figure 2: Complete overview of the 2.5D hierarchical alignment approach. The red block is the focus of this paper, where we aim at minimizing the registration error in 2D.

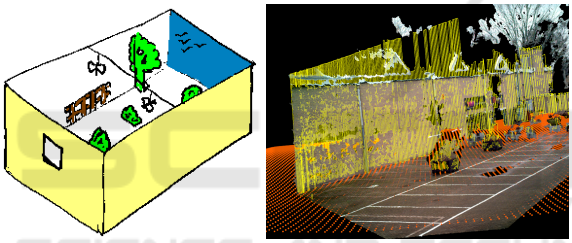

(a) (b)

Figure 3: (a) Diorama-box model representing the scene by superimposing flat objects on a ground plane. (b) Example visualization of the resulting model.

4 APPROACH

We introduce a diorama-box model, as illustrated in Figure 3, to be used as the historic 3D scene model in the alignment approach described in Section 3. This model is a simplification of the real world, where objects are modeled by flat planes that are perpendicular to the optical axis. This approach is especially suited for noisy depth data, such as captured by passive stereo cameras, which is insufficiently accurate for constructing a full 3D mesh of the scene. Figure 4 shows an example of such a point cloud as well as a zoom on one of the trees. This figure clearly demonstrates that it is not feasible to directly retrieve the 3D shape of the tree. Instead, we propose to approximate all objects above the ground surface by a planar structure, which is implemented efficiently by using the Stixel World algorithm (Pfeiffer, 2012) and projecting the stixels to 3D. In the Stixel World algorithm, the image is first divided into columns of fixed width. Based on the disparity estimates, each column is then split into vertically-stacked stixels, i.e. rectangular superpixels, using a maximum a-posteriori optimization. This process is solved efficiently with dynamic programming and results in a collection of stixels, each with a label to contain either ground or obstacle content. In this work, we are only interested in the obstacle stixels.

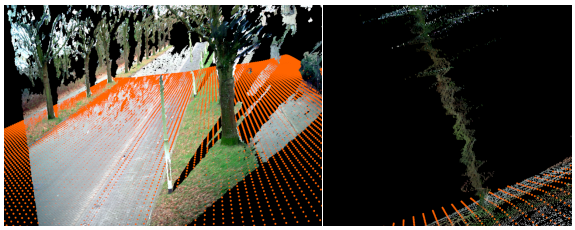

(a) (b)

Figure 4: (a) Example point cloud derived from stereo matching and (b) Zoomed view from the side of the tree, where depth inaccuracies deform its 3D shape.

4.1 Projecting Stixels to 3D

The Stixel World algorithm results in a set of rectangular super-pixels. As depth information is available, it can be used to map these super-pixels to 3D. However, directly projecting each stixel to 3D causes every stixel to be fronto-parallel, i.e. perpendicular to the optical axis. Obviously, this might not correspond to the actual orientation of the objects being modeled. Therefore, we slant each 3D stixel to better represent the actual objects. Stixel slanting is conceptually visualized in Figure 5. This slanting improves the model accuracy when rendering to a different viewpoint. The degree of slanting for each stixel is obtained through a least-squares plane fit on the disparity values within the stixel.

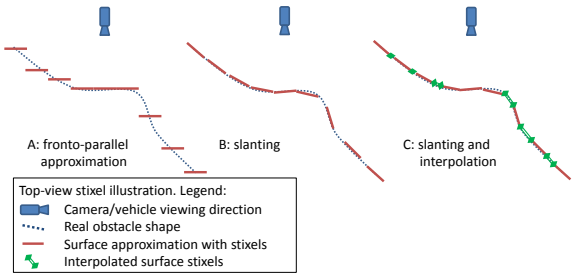

Figure 5: Conceptual visualization of stixel slanting and interpolation. Slanting ensures that the stixels follow the actual shape of the object more accurately, while interpolation fills the gaps between the 3D stixels.

4.2 3D Stixel Interpolation

Although stixels connect in 2D, they do not necessarily connect in 3D for two reasons. First, looking from the camera point-of-view, camera rays diverge, meaning adjacent pixels may map to world points, which are far apart. Second, as each stixel is assigned a slanting orientation, the stixel boundaries may not lie at the same depth. This causes holes in the 3D model when viewed from a different camera pose, as depicted in Figure 6(a). This figure clearly shows that holes appear, when projecting the 3D stixels to a different viewpoint without interpolation.

To counter this effect, we interpolate between adjacent stixels as shown in Figure 5, where we add a new stixel that connects two adjacent stixels, if they are sufficiently close to each other. The effect on the aligned image is shown in Figure 6(b).

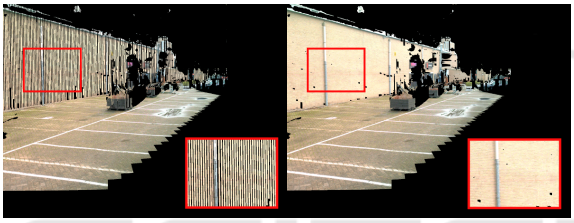

(a) (b)

Figure 6: Resulting aligned image (a) without stixel interpolation and (b) with stixel interpolation, when rendered to a synthetic viewpoint.

Although computing the stixel model at a lower resolution may decrease the number of holes in the resulting synthesized image, this would significantly decrease the capability to model thin objects. Therefore we consider the proposed stixel interpolation better suited to reduce holes, especially because the additional computation time is negligible.

4.3 Rejecting Invalid Pixels

In order to capture thin objects inside a stixel, we choose thin stixels with a width of only 7 pixels. It may still occur that an object only partially covers a stixel, since the horizontal grid is fixed. The resulting stixel may therefore contain both foreground and background pixels. Figure 7(a) shows an example of background pixels that are incorrectly treated as part of the tree. To correct for such errors, we adapt the texture map prior to projecting it onto the 3D model. Here, we label all pixels inside a stixel that do not satisfy the estimated slanting orientation, to be invalid. The invalid background pixels are then removed and replaced by black pixels in the aligned 2D image (Figure 7(b)).

(a) (b)

Figure 7: (a) Aligned image part where background pixels are contained inside a stixel and (b) the same image when pixels that do not satisfy the slanting orientation are set to invalid. This example uses wider stixels for visualization purposes.

5 EXPERIMENTS & RESULTS

The proposed registration approach using the box-diorama model has been validated on two separate datasets. The first dataset features many slanted surfaces, such as shown in Figure 6. The purpose of this dataset is to specifically evaluate the added value of our stixel slanting and interpolation adaptations within the proposed registration approach. Next, an additional dataset was recorded that features different lateral displacements, in order to evaluate the effect of viewpoint differences between the live and historic recordings.

To validate the proposed registration approach, we evaluate it on pairs of videos, which were recorded in both urban and industrial environments. Each video pair features a historic recording and a live recording of the same scene, acquired at a different moment in time. These videos were recorded under realistic conditions, by mounting the entire system on our driving prototype vehicle. This prototype (Figure 8) features a high-resolution stereo camera (1920×1440 pixels) as well as a GPS/IMU device for accurate georeferencing of all recorded images. While driving, live and historic images featuring the same scene from different viewpoints are paired using GPS position and vehicle orientation. Next, depth measurements are obtained through disparity estimation, yielding 3D information for both the live and historic scene. At this point, the baseline alignment approach (Section 3) is applied, which also includes the proposed 3D scene model (Section 4).

5.1 Performance Metrics

As this work aims at registering the live and historic images in 2D, we measure the alignment error bet-

Figure 8: Prototype vehicle used for our experiments, featuring a stereo camera with 1920×1440 pixel resolution and a GPS/IMU positioning system for georeferencing the images.

ween the live image and the aligned historic image. For the first dataset, we have manually annotated approximately 360 characteristic points in the set of live images, after which the exact same points were annotated in the registered historic images for every experiment. This resulted in a total of 1,800 manually annotated points for our first dataset. For the second dataset, we manually annotated 130 points for each displacement, resulting in a total of 650 annotations for this dataset. We employ the Euclidean distance (in pixels) between the annotated points in the live and registered images as a metric for the alignment accuracy of the proposed registration approach, including the box-diorama model.

The registration accuracy is defined as the percentage of annotations with an alignment error up to 5 pixels on images having 1920×1440 pixels. All presented results are based on the initial registration up to and including Stage 3 of the registration approach in Figure 2.

5.2 Evaluation

Figure 9 shows the registration accuracy when the proposed diorama-box model is used as a 3D model for scene alignment on our first dataset. Even without any post-processing, we achieve an accuracy of 90% after initial alignment. When slanting is not considered, the stixel interpolation improves the registration accuracy from 90% to 93%. The stixel slanting further improves the accuracy to 96%. This is also reflected in Figure 10, which even shows that most annotations have an alignment error below 2 pixels. Moreover, Figure 9 shows that already 79% of all annotations have an alignment error of 1 pixel or less on our first dataset.

Figure 10 portrays the histograms of the alignment errors. The reader may wonder about the 15+ pixel registration errors in the figure. These are mostly anno-

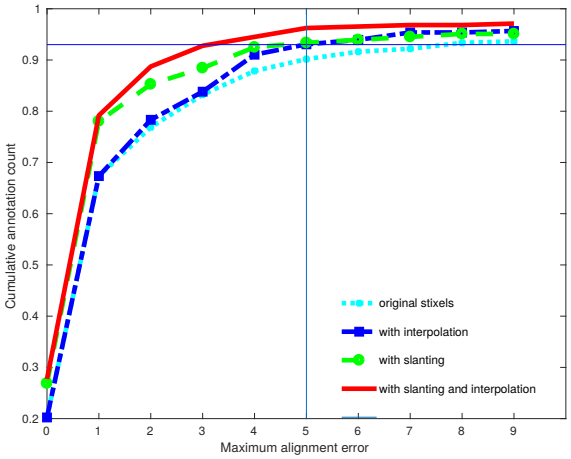

Figure 9: Registration accuracy plotted against the maximum alignment error, showing the cumulative amount of annotations satisfying a certain maximum alignment error.

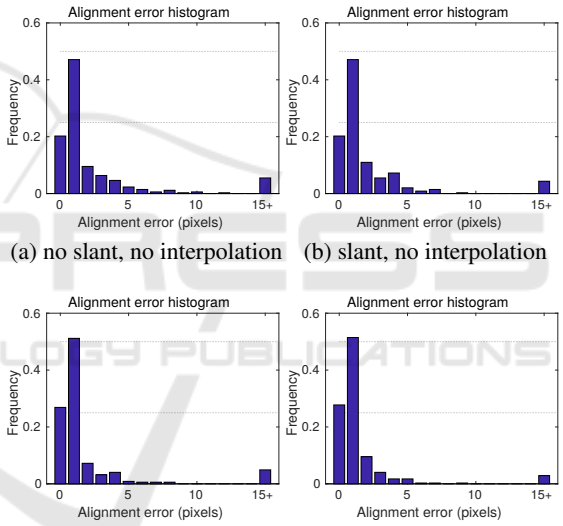

(a) no slant, no interpolation (b) slant, no interpolation

(c) no slant, interpolation (d) slant and interpolation

Figure 10: Alignment error histograms when the 3D model from Section 4 uses (a) stixels without slanting or interpolation, (b) stixels with slanting but without interpolation, (c) without slanting but with interpolation, (d) with both stixel slanting and interpolation.

tated points that could not be registered, because that specific part of an object was not covered by a stixel, or because no reliable depth data was available in that area. Such 'missing' points are assigned to the 15+ bin.

5.3 Effect of Lateral Displacement

This experiment is performed on the second dataset, which features different lateral displacements, i.e. different offsets between the live and historic recording, perpendicular to the viewing direction. Such a

Table 1: Registration accuracy for different lateral displacements of the vehicle. In these experiments, we use annotations up to a distance of 50 m. Figure 11 shows typical registration examples for each lateral displacement.

	lateral 0cm	lateral 160cm	lateral 350cm	lateral 530cm	lateral 700cm
Proposed	97%	90%	71%	53%	20%

Table 2: Examples of the proposed registration for different lateral displacements. The first row illustrates the target images. The second and third row show the source images and their corresponding disparitiy maps, respectively. The fourth row portrays the aligned images as rendered using the proposed registration approach, where black denotes areas outside of the Field-of-View of the historic camera. Finally, the last row shows the alignment error histograms for a specific lateral displacement using all images in the dataset with that displacement.

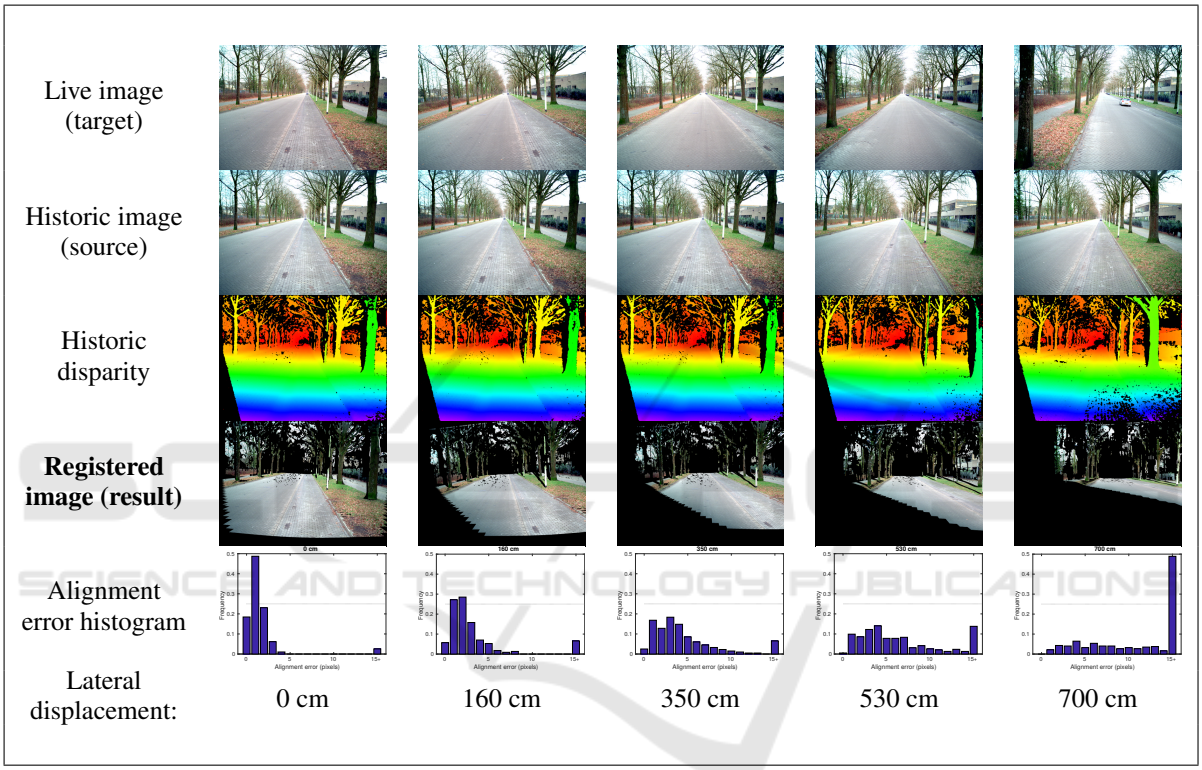

lateral displacement is caused by different driving trajectories between the live and historic recordings, e.g. keeping to a different driving lane. This causes significant viewpoint differences, as shown in Figure 1. The goal of this experiment is to identify the maximum allowed driving displacement during live operation.

Table 1 shows the registration accuracy for different lateral displacements for the proposed registration approach. We note that under ideal conditions, i.e. when the live and historic driving trajectory are almost identical, the proposed model is able to accurately align 97% of all annotated points. Even at displacements of 160 cm, the system is still able to align 90% of the points with an registration error of at most 5 pixels.

The decrease in registration accuracy for larger lateral displacements can be explained by the limited depth accuracy of our disparity estimation algorithm, which is outside the scope of this paper. At a distance of 40 meters, the smallest possible disparity step corresponds to a jump of 25 cm. Especially at larger distances, this leads to minor inaccuracies in the depth estimates of the stixels and hence the 3D positioning within our scene model. This is not a problem for small viewpoints variations (Column 2, Table 1), but when viewed from a significantly different viewpoint, the objects will be projected to a different coordinate in the registered image, i.e. will be misaligned.

The figures in Table 2 show typical examples of the input and output of our registration framework for different lateral displacements. Some holes in the registered images, such as part of the lantern pole missing in the second column of the table, are caused by

lack of any depth estimates in that area of the disparity map. Without depth data, no 3D object can be modeled at that location. In the case of the 700-cm displacement (Column 6), the only objects that remain in the overlapping Field-of-View lie too far away to be modeled with sufficient accuracy, hence the lower accuracy in Column 6 of Table 1.

We argue that the proposed model performs well for small to medium lateral displacements, e.g. up to and including 160 cm, while it is still able to align the majority of the scene for displacements of 350 cm, e.g. the typical distance between adjacent driving lanes. We note that displacements above 4 m exceed the operational range of the proposed registration system, although part of the scene can still be aligned for such extreme trajectory differences. Note from Table 2, Column 6, that the overlapping Field-of-View of the live and historic view has become too small and lies in the area where accurate depth information is no longer available.

5.4 Timing

Table 3 shows the execution times of the alignment approach when we extend the baseline method in Figure 2 with the proposed diorama-box model. Times are shown for both separate execution and under full CPU/GPU load, i.e. when running all pipestages simultaneously. Considering our HD+ stereo camera is restricted to 6 fps, the pipelined implementation operates at near real-time speed with 4 fps (including scheduling overhead).

Table 3: Execution times of the proposed registration approach with the box-diorama model included. Stage 1 and 2 involve the 3D Scene reconstruction from Figure 2, while Stage 3 both estimates the 3D transformation and simulates the live viewpoint (Block 2 and 3 in Fig. 2). The third column shows the execution times when the different pipeline stages are executed simultaneously, i.e. under full load. The (*) denotes that tasks can execute in parallel on CPU and GPU.

	t (ms)	t (ms) full load
Pipelined Stage 1:		
GPU: Depth estimation	90	153
Pipelined Stage 2		
CPU: Ground mesh*	130	200
GPU: 3D stixels mesh*	125	160
Pipelined Stage 3		
CPU: Find 3D pose diff	100	120
GPU: Viewpoint synthesis	30	46

6 DISCUSSION & RECOMMENDATIONS

We have introduced a diorama-box model for aligning images with viewpoint differences. The proposed work is part of a larger change detection system comparable to (van de Wouw et al., 2016), which aims at finding suspicious changes in the environment of undefined shape and nature, w.r.t. a previous recording. Scene alignment is a crucial aspect of this system, since without proper alignment the scene cannot be compared and changes may be missed. By extending the 3D ground-surface model of the baseline system with 3D objects, the operational range of the change detection system is significantly improved, where the analysis is no longer limited to the ground surface. Figure 11 shows the aligned images with and without the proposed model, clearly showing the improved alignment coverage, i.e. a larger part of the scene can be exploited for change detection.

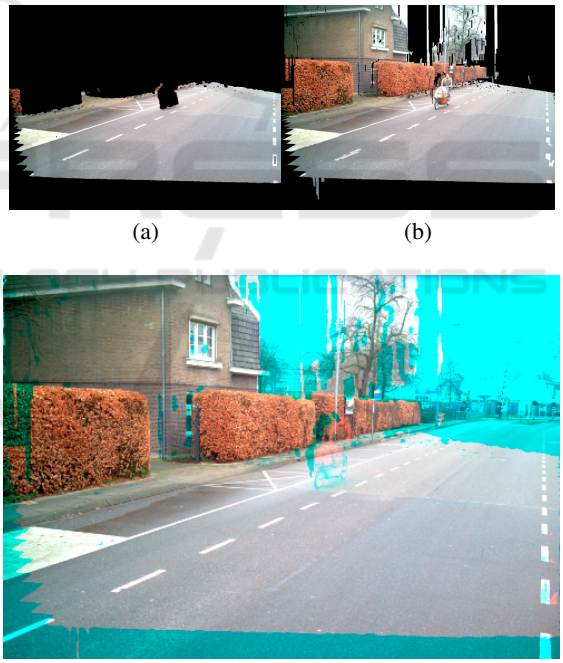

(a) (b)

(c)

Figure 11: Aligned images when using (a) ground-surface model from (van de Wouw et al., 2016), (b) proposed model including the 3D objects. Subfigure (c) shows an overlay of the live image (cyan) and the aligned historic scene (red).

Although the proposed work has similarities with the multi-view registration approaches discussed in Section 2, we cannot use the datasets introduced in their work. These datasets typically feature mono images from different viewpoint, whereas we need stereo images or a disparity map in our approach.

It was observed that rejecting invalid pixels within stixels occasionally results in small holes in the registered images at locations where no disparity estimate is available. Although such holes can mostly be avoided by using a morphological-closing filter prior to rejecting the pixels, some holes may persist. However, the downside of having small holes in the registered image did not outweigh the benefit of having a cleaner texture projection. We plan to look into guided-image filtering to prevent such holes and further refine the stixel boundaries in future work.

The current disparity estimation, which is outside the scope of this work, is noisy and has a very limited sub-pixel resolution. We hypothesize that a more expensive disparity estimation algorithm, increased baseline or zoom-lenses will improve the depth accuracy, which in turn will extend the operational range of the proposed 3D model.

7 CONCLUSION

We have introduced a diorama-box model for aligning images acquired from a moving vehicle. The proposed model extends the non-linear ground surface model (van de Wouw et al., 2016) with a model of the 3D objects in the scene. For this purpose, the Stixel World algorithm is used to segment the scene into super-pixels, which are projected to 3D to form an obstacle model. The consistency of the stixel-based model is improved by assigning a slanting orientation to each 3D stixel and by interpolating between the stixels to fill gaps in the 3D model. Consequently, registration accuracy is increased by 6%. As a further improvement of the algorithm, background pixels contained in object-related stixels are removed by checking their consistency with the stixel-slanting orientation. This improvement prevents ghosting effects, due to falsely projected background pixels.

The resulting alignment framework shows good results for typical driving scenarios, in which both live and historic recordings were acquired from the same driving lane. In this case, 96% of all manually annotated points are registered with an alignment error up to 5 pixels for images with a resolution of 1920×1440 pixels, where even 79% of the annotations have an error of unity pixel or lower. Even when driving in an adjacent lane, the system is able to accurately align 71% of all annotated points.

It was found that the disparity resolution of the depth map, i.e. the lack of sub-pixel accuracy, limits the accuracy of the 3D model, making it less effective for displacements above 4 meters. Nevertheless, the proposed work significantly improves the operational range of the real-time change detection system, which now covers the full 3D scene, instead of only the ground plane. Higher accuracies and/or performance of the change detection system can be achieved when important parameters are improved, such as lenses and/or a larger baseline, together with a more accurate depth estimation algorithm.

REFERENCES

Achanta, R., Shaji, A., Smith, K., Lucchi, A., Fua, P., and Susstrunk, S. (2012). Slic superpixels compared to state-of-the-art superpixel methods. *IEEE Trans. Pattern Anal. Mach. Intell.*, 34(11):2274–2282.

Broggi, A., Cattani, S., Patander, M., Sabbatelli, M., and Zani, P. (2013). A full-3d voxel-based dynamic obstacle detection for urban scenario using stereo vision. In *Intelligent Transportation Systems-(ITSC), 2013 16th International IEEE Conference on*, pages 71–76. IEEE.

Chauve, A. L., Labatut, P., and Pons, J. P. (2010). Robust piecewise-planar 3d reconstruction and completion from large-scale unstructured point data. In *2010 IEEE Computer Society Conference on Computer Vision and Pattern Recognition*, pages 1261–1268.

Cordts, M., Rehfeld, T., Enzweiler, M., Franke, U., and Roth, S. (2016). Tree-structured models for efficient multi-cue scene labeling. *IEEE Transactions on Pattern Analysis and Machine Intelligence*.

Felzenszwalb, P. F. and Huttenlocher, D. P. (2004). Efficient graph-based image segmentation. *International Journal of Computer Vision*, 59(2):167–181.

Labatut, P., Pons, J.-P., and Keriven, R. (2009). Robust and efficient surface reconstruction from range data. In *Computer graphics forum*, volume 28, pages 2275–2290. Wiley Online Library.

Lou, Z. and Gevers, T. (2014). Image alignment by piecewise planar region matching. *IEEE Transactions on Multimedia*, 16(7):2052–2061.

Maiti, A. and Chakravarty, D. (2016). Performance analysis of different surface reconstruction algorithms for 3d reconstruction of outdoor objects from their digital images. *SpringerPlus*, 5(1):932.

Natour, G. E., Ait-Aider, O., Rouveure, R., Berry, F., and Faure, P. (2015). Toward 3d reconstruction of outdoor scenes using an mmw radar and a monocular vision sensor. *Sensors*, 15(10):25937–25967.

Pfeiffer, D.-I. D. (2012). *The stixel world*. PhD thesis, Humboldt-Universität zu Berlin.

Salman, N. and Yvinec, M. (2010). Surface reconstruction from multi-view stereo of large-scale outdoor scenes. *International Journal of Virtual Reality*, 9(1):19–26.

Sanberg, W. P., Do, L., and de With, P. H. N. (2013). Flexible multi-modal graph-based segmentation. In *Advanced Concepts for Intelligent Vision Systems: 15th International Conference, ACIVS 2013, Poznań, Poland, October 28-31, 2013. Proceedings*, pages 492–503. Springer International Publishing.

Strom, J., Richardson, A., and Olson, E. (2010). Graph-based segmentation for colored 3d laser point clouds. In *Intelligent Robots and Systems (IROS), 2010 IEEE/RSJ International Conference on*, pages 2131–2136. IEEE.

Su, H. R. and Lai, S. H. (2015). Non-rigid registration of images with geometric and photometric deformation by using local affine Fourier-moment matching. *Proceedings of the IEEE Computer Society Conference on Computer Vision and Pattern Recognition*, 07-12-June:2874–2882.

van de Wouw, D. W. J. M., Dubbelman, G., and de With, P. H. N. (2016). Hierarchical 2.5-d scene alignment for change detection with large viewpoint differences. *IEEE Robotics and Automation Letters*, 1(1):361–368.

van de Wouw, D. W. J. M., Pieck, M. A., Dubbelman, G., and de With, P. H. (2017). Real-time estimation of the 3d transformation between images with large viewpoint differences in cluttered environments. *Electronic Imaging*, 2017(13):109–116.

Veksler, O., Boykov, Y., and Mehrani, P. (2010). Superpixels and supervoxels in an energy optimization framework. In *European conference on Computer vision*, pages 211–224. Springer.

Werlberger, M., Pock, T., and Bischof, H. (2010). Motion estimation with non-local total variation regularization. In *2010 IEEE Computer Society Conference on Computer Vision and Pattern Recognition*, pages 2464–2471.

Yamaguchi, K., McAllester, D., and Urtasun, R. (2014). *Efficient Joint Segmentation, Occlusion Labeling, Stereo and Flow Estimation*, pages 756–771. Springer International Publishing, Cham.

Zhang, G., He, Y., Chen, W., Jia, J., and Bao, H. (2016). Multi-Viewpoint Panorama Construction with Wide-Baseline Images. *IEEE Transactions on Image Processing*, 25(7):3099–3111.